

---

# Molecular Generative Adversarial Network with Multi-Property Optimization

---

Huidong Tang<sup>1</sup> Chen Li<sup>2</sup> Sayaka Kamei<sup>1</sup> Yoshihiro Yamanishi<sup>2</sup> Yasuhiko Morimoto<sup>1</sup>

## Abstract

Deep generative models, such as generative adversarial networks (GANs), have been employed for *de novo* molecular generation in drug discovery. Most prior studies have utilized reinforcement learning (RL) algorithms, particularly Monte Carlo tree search (MCTS), to handle the discrete nature of molecular representations in GANs. However, due to the inherent instability in training GANs and RL models, along with the high computational cost associated with MCTS sampling, MCTS RL-based GANs struggle to scale to large chemical databases. To tackle these challenges, this study introduces a novel GAN based on actor-critic RL with instant and global rewards, called InstGAN, to generate molecules at the token-level with multi-property optimization. Furthermore, maximized information entropy is leveraged to alleviate the mode collapse. The experimental results demonstrate that InstGAN outperforms other baselines, achieves comparable performance to state-of-the-art models, and efficiently generates molecules with multi-property optimization. The source code will be released upon acceptance of the paper.

## 1. Introduction

Modern human healthcare and well-being are intricately intertwined with the field of drug discovery, which seeks to uncover new chemical compounds with therapeutic effects. However, traditional drug discovery is a time-consuming and expensive endeavor, averaging a staggering 12 years and incurring a cost of 2.6 billion USD (Chan et al., 2019). To expedite the process and mitigate costs, artificial intelligence (AI) has garnered the attention of the pharmaceutical industry (Paul et al., 2021). Among the recent applications

of AI, deep generative models have demonstrated remarkable progress, as exemplified by DALL·E2 in the realm of computer vision and ChatGPT in natural language processing (NLP) (OpenAI, 2023). The adoption of such models has also become increasingly prominent in the field of drug discovery (Chen et al., 2018).

Molecular graphs (Shi et al., 2020) and simplified molecular input line entry systems (SMILES) strings (Weininger, 1988) constitute the two primary representations of molecules in deep generative models. However, generating molecules with desired chemical properties using such discrete representations is a non-trivial task. Most prior studies related to generative adversarial networks (GANs) (Yu et al., 2017; Guimaraes et al., 2017; De Cao & Kipf, 2018) typically update the generator by integrating the output probability of the discriminator with the chemical properties of generated molecules as a reward for reinforcement learning (RL), following the REINFORCE algorithm (Williams, 1992). Due to the inability of GANs to calculate rewards for partially generated molecules, Monte Carlo tree search (MCTS) is frequently utilized for sampling and completing molecules (Li et al., 2022). Unfortunately, the integration of RL algorithms with GANs further exacerbates the instability of the training process. Stabilizing MCTS demands a substantial number of samples, significantly lengthening the process (Li & Yamanishi, 2023).

Furthermore, most aforementioned studies on *de novo* molecular generation have focused on optimizing a single chemical property. However, in practical applications, it is often desirable to generate molecules that satisfy multiple chemical property constraints. In contrast to the former, multi-property optimization is highly complicated and challenging to achieve in nature. This is because the multi-property optimization task entails not only learning the semantic and syntactic rules of molecules to generate valid molecules from scratch but also finding pathways to optimize the distribution of chemical properties during the process (Barshatski et al., 2021). For example, molecules exhibiting both drug-likeness and dopamine receptor (DRD2) activity represent only 1.6% of the generated molecules (Jin et al., 2019). Therefore, employing deep generative models for *de novo* molecular generation with multi-property optimization holds significance to the drug discovery industry (Barshatski & Radinsky, 2021).

---

<sup>1</sup>Graduate School of Advanced Science and Engineering, Hiroshima University, Hiroshima, Japan <sup>2</sup>Graduate School of Informatics, Nagoya University, Nagoya, Japan. Correspondence to: Huidong Tang <d216083@hiroshima-u.ac.jp>, Chen Li <li.chen.z2@a.mail.nagoya-u.ac.jp>.

Inspired by the previous studies in (De Cao & Kipf, 2018; Tang et al., 2023), this study introduces a novel GAN based on actor-critic RL with instant rewards (IR) and global rewards (GR), called InstGAN, to generate molecules at the token-level with multi-property optimization. Specifically, the generator is constructed using a long short-term memory (LSTM) that generates SMILES strings in an autoregressive manner. The discriminator quantifies each token based on SMILES substrings produced by the generator. To enhance the ability of the discriminator to quantize tokens, a bidirectional LSTM (Bi-LSTM) is chosen as the discriminator. Additionally, multiple property prediction networks with the same structure as the discriminator predict the corresponding property scores for each token as well. Subsequently, the scores of discriminator and property prediction networks, along with their global-level scores, serve as rewards for RL. To expedite the training process and facilitate its application to extensive chemical databases, an IR calculation based on actor-critic RL is proposed to update the generator. Furthermore, the maximized information entropy (MIE) is included in the loss function for generator updates to mitigate mode collapse and enhance molecular diversity. The main contributions are as follows:

- **Novel reward calculation:** This study proposes an actor-critic RL-based approach to calculate IR and GR for molecular generation with multi-property optimization.
- **Scalability for chemical property optimization:** InstGAN exhibits versatile scalability, enabling flexible expansion from single-property to arbitrary multi-property optimized molecular GAN.
- **Superior performance:** Experimental results validate that InstGAN outperforms other baselines, achieves comparable performance to state-of-the-art (SOTA) models, and demonstrates the ability to generate molecules with multi-property optimization in a fast and efficient manner.

## 2. Related Work

### 2.1. Variational autoencoder (VAE)-based Models

Two VAE variants, Character-VAE and Grammar-VAE (Kusner et al., 2017), integrate parse trees with VAEs to facilitate the generation of syntactically valid molecules. However, due to ignoring the semantic information of the molecular representations, the correlation between the training set and the generated molecules cannot be guaranteed. In contrast, Syntax-VAE (Dai et al., 2018) ensures that the generated molecules are both syntactically valid and semantically meaningful. JT-VAE (Jin et al., 2018) adopts a two-step VAE approach, first generating tree-structured scaffolds based on chemical substructures

and then combining these outputs into complete molecules using a graph message-passing network (Dai et al., 2016; Gilmer et al., 2017). Nonetheless, a major limitation of VAEs is the typically limited size of the latent space, which may restrict the capacity to produce highly realistic molecules.

### 2.2. Flow-based Models

GraphAF (Shi et al., 2020) utilizes a flow-based autoregressive model to generate molecular graphs. GraphDF (Luo et al., 2021) incorporates invertible modulo shift transforms to connect discrete latent variables with graph nodes and edges, resulting in the generation of molecular graphs. MoFlow (Zang & Wang, 2020) adopts a Glow-based model (Kingma & Dhariwal, 2018) to generate chemical bonds as graph edges and employs a graph conditional flow to subsequently generate atoms as graph nodes, followed by posthoc validity correction. GraphCNF (Lippe & Gavves, 2021) falls under the category of flow-based models, commonly applied in various data domains. In molecular graph generation, GraphCNF leverages flow-based techniques to address the unique challenges associated with generating molecular graphs. However, flow-based models generally exhibit two notable limitations: the computation of the Jacobian matrix is time-consuming, often requiring approximations, and the necessity for network invertibility imposes constraints on their representational capacity (Zhang et al., 2021).

### 2.3. Diffusion-based Models

Recently, diffusion models have found application in the domain of molecular generation, where they are being utilized to tackle the intricate challenges associated with generating molecular structures that adhere to specific chemical and property constraints. DiGress (Vignac et al., 2023) iteratively refines noisy graphs by adding or removing edges and adjusting categories, which results in the generation of molecular graphs with node and edge attributes suitable for classification. GDSS (Jo et al., 2022) and D2L-OMP (Guo et al., 2023) are the two SOTA models in the realm of molecular generation. GDSS skillfully captures the joint distribution of molecular nodes and edges, generating molecular replicas closely aligned with the training distribution. D2L-OMP generates a hybrid Gaussian distribution by employing diffusion on two structural levels: molecules and molecular fragments. This hybrid Gaussian distribution is then utilized in the reverse denoising process.

### 2.4. GAN-based Models

SeqGAN (Yu et al., 2017) pioneered the incorporation of MCTS-based RL into GAN architecture, specifically designed to handle discrete text. This innovation has

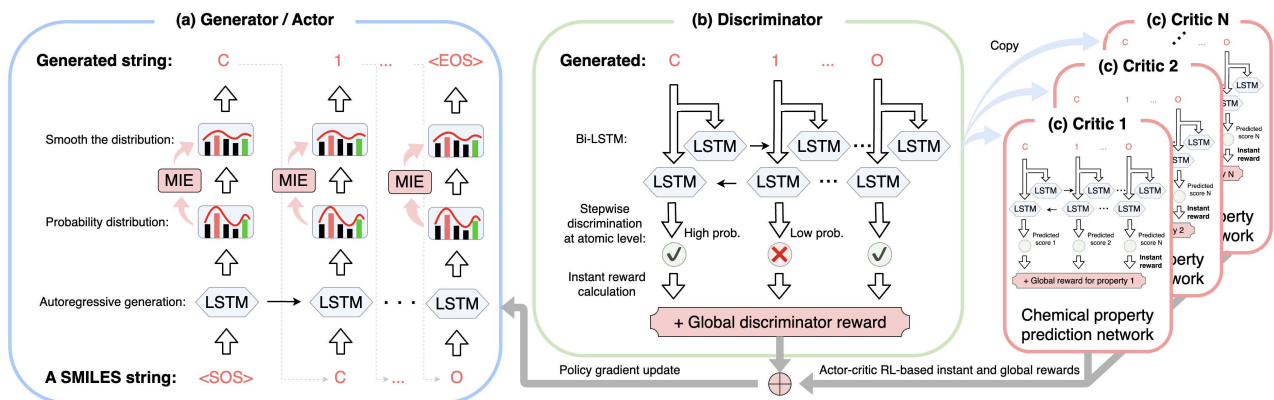


Figure 1. The architectural overview of InstGAN comprises three main substructures. **(a) The generator**, featuring an LSTM, produces tokens in an autoregressive manner at each time step. MIE is employed to enhance the likelihood of sampling different tokens, smoothing the output probability distribution for the generator. **(b) The discriminator**, a Bi-LSTM, scores generated tokens based on both forward and backward at each time step, enabling semantic and syntactic discrimination at the token-level. Higher probabilities are assigned to likely generated tokens, while those with errors receive lower probabilities. The average of all-token probabilities assesses overall generation quality from a global perspective. **(c) Multiple pretrained chemical property prediction networks**, labeled Critic 1 to Critic  $N$ , have the same structure as the discriminator. They predict various chemical properties for each token of a generated SMILES string. Similarly, the sum of stepwise scores is averaged to provide a global property score for the entire SMILES string. Finally, scores from the discriminator and critics serve as rewards in the actor-critic RL algorithm, co-updating the generator via the policy gradients.

inspired various studies on molecular generation using GANs. MolGAN (De Cao & Kipf, 2018) introduces an implicit, likelihood-free discrete GAN for generating small molecular graphs. However, MolGAN faces an overfitting problem, leading to less than 5% uniqueness in the generated molecules. ORGAN (Guimaraes et al., 2017) integrates domain-specific knowledge as rewards for generating SMILES strings through the MCTS-based RL algorithm. TransORGAN (Li et al., 2022) leverages a transformer architecture to capture semantic information and employs variant SMILES technique for syntax rule learning. SpotGAN (Li & Yamanishi, 2023) adopts a first-decoder-then-encoder transformer model for generating SMILES strings from a given scaffold. However, the use of MCTS-based RL in GANs often demands a substantial number of samples for training stability, making it impractical for extensive chemical databases. EarlGAN (Tang et al., 2023), while capable of generating valid molecules on large chemical databases, lacks the ability to optimize chemical properties, particularly multiple properties simultaneously. This study introduces an actor-critic RL-driven GAN that employs IR and GR to enhance the efficiency of learning semantic and syntactic rules in SMILES strings. Furthermore, our other goal is to identify pathways to optimize the generation of molecules across a broad spectrum of chemical properties.

### 3. Model

Figure 1 illustrates the overall architecture of InstGAN and highlights the three key substructures (i.e., the generator, discriminator, and multiple chemical property prediction networks) that are crucial for generating molecules with multi-property optimization from scratch.

Formally, let  $G_\theta$  and  $D_\phi$  represent the generator and discriminator of InstGAN with parameters  $\theta$  and  $\phi$ , respectively.  $\mathcal{S}_{1:T} = [s_1, \dots, s_T]$  denotes a SMILES string with a sequence length of  $T$ . Then, the min-max optimization procedure (Goodfellow et al., 2014) is as follows:

$$\min_{\theta} \max_{\phi} V(G_\theta, D_\phi) = \mathbb{E}_{\mathcal{S} \sim p_r(\mathcal{S})} [\log D_\phi(\mathcal{S})] + \mathbb{E}_{\mathcal{S} \sim p_\theta(\mathcal{S})} [\log(1 - D_\phi(\mathcal{S}))], \quad (1)$$

where  $p_r(\cdot)$  and  $p_\theta(\cdot)$  represent the distributions of training SMILES strings and generated sequences, respectively. Following a similar approach to NLP methods (de Masson d’Autume et al., 2019; Fedus et al., 2018), InstGAN utilizes an autoregressive generator and discriminator. Notably, this design allows for the allocation of dense rewards at the token-level. See Appendix A for more details on InstGAN’s generator and discriminator.

#### 3.1. Token-Level Critics

Unlike graph-based approaches, molecular generative models relying on SMILES strings often face challenges in ensuring high validity due to the intricacies of checking valence during the autoregressive generation process. Typi-

cally, invalid SMILES strings may arise from mismatched tokens, requiring the removal or replacement of other suitable tokens to restore validity. Therefore, a crucial aspect of addressing this issue lies in the meticulous assessment of SMILES strings at the token-level.

**Token-level discriminator.** In InstGAN, the generator employs an autoregressive process to produce SMILES strings, serving as inputs for the discriminator. Diverging from traditional discriminators, InstGAN performs token-level discrimination for each generated token. Specifically, with a Bi-LSTM, let  $\vec{S}_{1:t}$  and  $\overleftarrow{S}_{t:T}$  represent the forward and backward SMILES substrings, respectively. The discriminator calculates the probability  $r_t^D$  that it deems the  $t$ -th token  $\tilde{s}_t$  of the SMILES string as true. The calculation is formulated as follows:

$$r_t^D = D_\phi(\tilde{s}_t | \vec{S}_{1:t}, \overleftarrow{S}_{t:T}). \quad (2)$$

To assess the overall validity of the entire SMILES string, we calculate the global discriminator score as follows:

$$r_{1:T}^D = \frac{1}{T} \sum_{t=1}^T r_t^D. \quad (3)$$

**Token-level property prediction networks.** The chemical property prediction networks are replicated from the discriminator and share the same structure. In the pretraining phase, the entire SMILES string serves as input, and the networks utilize the corresponding property values of the complete SMILES string as labels for the chemical properties of its tokens at each step. In the training phase of InstGAN, these networks calculate both instant and global chemical properties of the generated SMILES string. Collaborating with the discriminator, they contribute to updating the generator using actor-critic RL-based rewards.

### 3.2. Instant and Global Reward Calculation

Following the actor-critic RL algorithm, the generator functions as the actor network responsible for action selection, while the discriminator, along with the property prediction networks, serves as the critic for reward calculation. However, in contrast to the traditional actor-critic RL algorithm (Konda & Tsitsiklis, 1999), which calculates the reward at the last time step  $T$ , we compute the reward for each token of the discriminator as follows:

$$R_t^D = 2r_t^D - 1 + W^D r_{1:T}^D, \quad (4)$$

where  $W^D$  represents the weight assigned to the discriminator’s GR. Similarly, the reward of the property prediction networks can be calculated and denoted as  $R_t^{C_i}$ ,  $i \in [1, 2, \dots, N]$ , and  $N$  indicates the number of chemical properties to be optimized. Subsequently, the overall

---

#### Algorithm 1 Training procedure of InstGAN.

---

- 1: **Data:** a SMILES dataset  $\mathcal{D}_{real}$
  - 2: **Initialization:** generator:  $G_\theta$ , discriminator:  $D_\phi$ , property prediction networks:  $C_{\varphi_i}^i, i \in [1, \dots, N]$
  - 3: Generate a dataset  $\mathcal{D}_{fake}$  from scratch
  - 4: // Pretrain the discriminator
  - 5: **for**  $k = 1 \rightarrow d$ -steps **do**
  - 6:   Update  $D_\phi$  on  $\mathcal{D}_{real}$  and  $\mathcal{D}_{fake}$
  - 7: **end for**
  - 8: // Pretrain the generator
  - 9: **for**  $k = 1 \rightarrow g$ -steps **do**
  - 10:   Update  $G_\theta$  on  $\mathcal{D}_{real}$
  - 11: **end for**
  - 12: // Pretrain property networks
  - 13: **for**  $i = 1 \rightarrow N$  **do**
  - 14:   **for**  $k = 1 \rightarrow p$ -steps **do**
  - 15:     Update  $C_{\varphi_i}^i$  on  $\mathcal{D}_{real}$
  - 16:   **end for**
  - 17: **end for**
  - 18: // Multi-property optimization
  - 19: **for**  $k = 1 \rightarrow$  steps **do**
  - 20:    $G_\theta$  updates the generated dataset  $\mathcal{D}_{fake}$
  - 21:   Update  $D_\phi$  and  $C_{\varphi_i}^i$
  - 22:    $D_\phi$  discriminates between  $\mathcal{D}_{real}$  and  $\mathcal{D}_{fake}$  and outputs the IR and GR
  - 23:    $C_{\varphi_i}^i$  calculates the IR and GR for chemical properties
  - 24:   Update  $G_\theta$  based on the rewards
  - 25: **end for**
- 

reward for chemical properties is represented as follows:

$$R_t^C = \sum_{i=1}^N W_{C_i} R_t^{C_i}. \quad (5)$$

Here,  $W_{C_i}$  denotes the weight assigned to the  $i$ -th chemical property prediction network. Finally, the total reward  $R_t$  at time step  $t$  can be calculated as

$$R_t = (1 - \lambda)R_t^D + \lambda R_t^C, \quad (6)$$

where  $\lambda$  represents a hyperparameter that balances the trade-off between the GAN and RL components.

### 3.3. Objective Function

In the iterative adversarial process, the generator is updated by the MCTS-based RL algorithm through the sampling of numerous samples, leading to a computational training process. In contrast, InstGAN utilizes rewards derived from the actor-critic RL algorithm and MIE for the calculation. The overall loss function for the generator is calculated as

$$\mathcal{L}_\theta = \mathcal{L}_{RL} + \beta \mathcal{L}_{MIE}, \quad (7)$$



Table 1. Statistical descriptions of ZINC and ChEMBL datasets.

| Dataset | MaxL | MinL | AvgL | QED  | logP | SA   | DRD2 |
|---------|------|------|------|------|------|------|------|
| ZINC    | 109  | 9    | 44   | 0.73 | 0.56 | 0.56 | 0.24 |
| ChEMBL  | 116  | 10   | 47   | 0.57 | 0.67 | 0.62 | 0.25 |

\* MaxL, MinL, and AvgL indicate the maximum, minimum, and average length of the SMILES strings.

where  $\mathcal{L}_{RL}$  and  $\mathcal{L}_{MIE}$  represent the loss functions of RL and MIE, respectively, with  $\beta$  serving as the trade-off parameter between them. In accordance with the policy gradient,  $\mathcal{L}_{RL}$  is calculated by minimizing the expected reward score:

$$\mathcal{L}_{RL} = -\frac{1}{T} \sum_{\mathbf{S}_{1:T}} (R_t - b_t) \log p_{\theta}(s_t | \mathbf{S}_{1:t-1}), \quad (8)$$

where  $b_t$  denotes the baseline using the global moving-average rewards (Sutton & Barto, 2018), which is calculated using both the mean reward  $\bar{R}$  across the current batch and the previous baseline  $b_{t-1}$ . The calculation is as follows:

$$b_t = (1 - \alpha)\bar{R} + \alpha b_{t-1}. \quad (9)$$

Here,  $\alpha$  denotes a smoothing factor. To encourage the generator to sample tokens with probabilities other than the highest, MIE  $\mathcal{L}_{MIE}$  is incorporated into the generator’s loss function. This addition serves to smooth the probability distribution, mitigating the mode collapse problem and promoting diversity in generating molecules.

$$\mathcal{L}_{MIE} = \frac{1}{T} \sum_{\mathbf{S}_{1:T}} \sum_{v=1}^V p_{\theta}(s_t^v) \log p_{\theta}(s_t^v), \quad (10)$$

where  $V$  represents the size of chemical vocabulary.

Algorithm 1 outlines the training procedure for InstGAN with multi-property optimization. The generator, discriminator, and multiple chemical property prediction networks are first pretrained. Then, the generator is trained to generate a dataset. Afterward, the discriminator and critics are updated using both real and generated SMILES strings. Finally, the IR and GR are calculated to update the generator.

## 4. Experiments

### 4.1. Experimental Setup

**Datasets.** The performance of InstGAN was validated through experiments on two widely used chemical datasets: ZINC (Irwin et al., 2012) and ChEMBL (Gaulton et al., 2017). The ZINC dataset contains 250,000 drug-like molecules. The ChEMBL dataset includes approximately 1.6 million molecules, with each having a median of 27 and a maximum of 88 heavy atoms.

**Chemical properties.** The molecular property optimization focused on the following chemical properties:

- **Drug-likeness (QED)** is a metric that quantifies the likelihood of a molecule being a successful drug based on favorable molecular characteristics (Bickerton et al., 2012).
- **Solubility (logP)** measures how well a molecule dissolves in lipid versus aqueous environments, quantified as the Log of the partition coefficient (Comer & Tam, 2001).
- **Synthesizability (SA)** is defined by the synthetic accessibility score, evaluating the ease with which a molecule can be synthesized (Ertl & Schuffenhauer, 2009).
- **Dopamine receptor D2 (DRD2)** is a central nervous system G protein-coupled receptor that is essential for dopamine-mediated signaling (Olivecrona et al., 2017).

**Metrics.** The assessment of the molecular generation follows criteria outlined in (Li & Yamanishi, 2023). **Validity** is assessed by the proportion of chemically valid molecules among all generated ones, validated practically using the RDKit tool (Landrum, 2013). **Uniqueness** is determined by the proportion of non-duplicated molecules among all valid ones. **Novelty** is defined as the proportion of unique molecules not present in the training set. **Total** is the ratio of novel molecules to all generated ones. **Diversity** is calculated as the average Tanimoto distance (Rogers & Tanimoto, 1960) between the Morgan fingerprints (Cereto-Massagué et al., 2015) of novel molecules (refer to Appendix B).

All these properties and evaluation metrics are normalized to a range of  $[0, 1]$ , where a higher score indicates better performance. Table 1 provides statistics of the datasets.

**Hyperparameters.** For pretraining, the learning rate was set to  $2e-4$ . InstGAN was pretrained with up to 60,000 steps, the batch size was 1024, the MIE trade-off  $\beta$  was set to  $1e-3$ , and the GR weight  $W^D$  was  $7.1e-5$ . For multi-property optimization, QED, logP, and SA were used as the desired chemical properties, and the weights of  $W_{C_i}$  were set to 0.4, 0.3, and 0.3. The learning rate was set to  $5e-6$ , and the GAN was trained with a maximum of 5,000 steps with a batch size of 256. Additionally, the dropout rate was 0.1, and the gradient clippings range was from -0.1 to 0.1. The MIE trade-off  $\beta$  was set to  $2.2e-2$ , the GR weight  $W^D$  was  $1e-5$ , and the smoothing factor  $\alpha$  was set to 0.9. The L2 coefficient for the critics was  $1e-6$ . The maximum string length of generated SMILES was fixed at 49. Evaluations were conducted every 100 steps, with 10,000 samples generated. All experiments were performed within the NVIDIA GeForce RTX 3090 GPU environment.

Table 2. Comparison results of InstGAN with various baseline models for chemical property optimization on the ZINC dataset.

|                 | Model                               | Validity (%) $\uparrow$ | Uniqueness (%) $\uparrow$ | Novelty (%) $\uparrow$ | Total (%) $\uparrow$ |
|-----------------|-------------------------------------|-------------------------|---------------------------|------------------------|----------------------|
| VAE-based       | RNN-Attention (Dollar et al., 2021) | 71.57                   | 99.94                     | 100.0                  | 71.53                |
|                 | TransVAE (Dollar et al., 2021)      | 25.39                   | 99.96                     | 100.0                  | 25.38                |
|                 | Character-VAE (Kusner et al., 2017) | 86.65                   | 81.21                     | 26.36                  | 18.55                |
|                 | Grammar-VAE (Kusner et al., 2017)   | 91.91                   | 77.24                     | 11.90                  | 8.45                 |
|                 | JT-VAE (Jin et al., 2018)           | 100.0                   | 19.75                     | 99.75                  | 19.70                |
| Flow-based      | GraphAF (Shi et al., 2020)          | 68.00                   | 99.10                     | 100.0                  | 67.39                |
|                 | GraphDF (Luo et al., 2021)          | 89.03                   | 99.16                     | 100.0                  | 88.28                |
|                 | MoFlow (Zang & Wang, 2020)          | 81.76                   | 99.99                     | 100.0                  | 81.75                |
|                 | GraphCNF (Lippe & Gavves, 2021)     | 63.56                   | 100.0                     | 100.0                  | 63.56                |
| Diffusion-based | GDSS (Jo et al., 2022)              | 97.01                   | 99.64                     | 100.0                  | 96.66                |
|                 | D2L-OMP (Guo et al., 2023)          | 97.51                   | 99.88                     | 100.0                  | 97.39                |
| GAN-based       | ORGAN (Guimaraes et al., 2017)      | 67.96                   | 98.20                     | 98.39                  | 65.66                |
|                 | MolGAN (De Cao & Kipf, 2018)        | 95.30                   | 4.30                      | 100.0                  | 4.10                 |
|                 | TransORGAN (Li et al., 2022)        | 74.31                   | 91.79                     | 100.0                  | 68.21                |
|                 | SpotGAN (Li & Yamanishi, 2023)      | 93.26                   | 92.78                     | 92.75                  | 80.25                |
| InstGAN         | Pretrain (Average)                  | 95.45                   | 98.63                     | 99.71                  | 93.87                |
|                 | Single property (QED)               | 97.89                   | 98.31                     | 99.69                  | 95.94                |
|                 | Single property (logP)              | 96.65                   | 98.42                     | 99.93                  | 95.05                |
|                 | Single property (SA)                | 97.46                   | 98.59                     | 99.75                  | 95.85                |
|                 | Multi-properties (QED, logP, SA)    | 97.71                   | 98.71                     | 99.64                  | 96.10                |

\* The values in the gray cells indicate the maximum scores in the respective columns.

## 4.2. Evaluation Results

**Comparison results with baselines.** Table 2 compared the results of InstGAN with various baseline models (including VAE-, flow-, diffusion-, and GAN-based models) for chemical property optimization on the ZINC dataset. To ensure a fair comparison, InstGAN was pretrained several times, and the average results are presented. Additional details on these multiple pretraining sessions are provided in Appendix C. For VAE-based models, although RNN-Attention and TransVAE generated molecules that were highly unique and novel, their validity (i.e., < 71.6%) was significantly lower compared to InstGAN. InstGAN outperformed Character-VAE and Grammar-VAE in all metrics. Although JT-VAE exhibited high validity and novelty, the uniqueness was only 19.75%, significantly lower than that of InstGAN. For flow-based models, despite exhibiting high uniqueness and novelty, their validity was lower, specifically less than 89.03%, which significantly trails behind InstGAN. InstGAN demonstrated comparable performance to SOTA diffusion models GDSS and D2L-OMP. All models, including pretraining and tasks involving single properties (QED, logP, SA), as well as multi-property tasks (QED, logP, SA), achieved an overall score surpassing 93.87%. Among GAN-based models, while MolGAN and TransORGAN exhibited a novelty of 100.0%, their validity and uniqueness fell significantly lower than Inst-

GAN. Specifically, MolGAN demonstrated a mere 4.3% uniqueness, and TransORGAN exhibited a validity of only 74.31%. ORGAN’s validity stood at 67.96%, markedly lower than InstGAN’s impressively high validity exceeding 95.45%. Furthermore, InstGAN outperformed SpotGAN in terms of validity, uniqueness, novelty, and total score, with the highest overall performance. InstGAN was trained for single- and multi-property optimization. In single-property optimization, InstGAN was trained individually using QED, logP, and SA. In multi-property optimization, these three properties were used to jointly train InstGAN. The validity, uniqueness, novelty, and total score all reached up to 93.87%. Overall, while InstGAN generated molecules from less informative SMILES strings compared to graph-based models, it surpassed VAE-, flow-, and GAN-based baselines and demonstrated comparable performance to SOTA diffusion models. This showcases InstGAN’s robust capability in molecular generation, excelling in both single- and multi-property optimization.

**Property optimization.** Owing to the diverse sequence representations in SMILES strings, they inherently introduce more noise compared to molecular graphs. Furthermore, as molecular graphs typically contain more detailed information, including atoms, chemical bonds, and valences, the task of molecular generation based on SMILES

Table 3. Multi-property assessment and comparison of the top-k generated molecules.

| Model (Property)      | Top-1 | Top-1000 | Top-2000 | Top-4000 | Top-6000 | Top-8000 |
|-----------------------|-------|----------|----------|----------|----------|----------|
| GraphAF (QED)         | 0.94  | 0.57     | -        | -        | -        | -        |
| GDSS (QED)            | 0.94  | 0.85     | -        | -        | -        | -        |
| MoFlow (QED)          | 0.93  | 0.78     | -        | -        | -        | -        |
| D2L-OMP (QED)         | 0.95  | 0.85     | -        | -        | -        | -        |
| <b>InstGAN (QED)</b>  | 0.95  | 0.93     | 0.92     | 0.90     | 0.88     | 0.86     |
| <b>InstGAN (logP)</b> | 1.00  | 0.89     | 0.85     | 0.81     | 0.78     | 0.74     |
| <b>InstGAN (SA)</b>   | 1.00  | 0.99     | 0.98     | 0.96     | 0.94     | 0.92     |

strings is more challenging. As illustrated in Table 2, InstGAN performed well in molecular generation in all evaluation metrics. InstGAN obtained almost 100% novelty in multi-property optimization, with validity and uniqueness exceeding 97.7%. InstGAN’s ability to excel in learning both semantic and syntactic features within SMILES strings is the key contributing factor to this achievement. This achievement surpassed the capabilities of all other models that rely on SMILES strings for chemical property optimization.

Table D.1 and Table 3 show the top-k property scores for the single- and multi-property optimization of the generated molecules, respectively. In single-property optimization, InstGAN enhanced all targeted chemical properties. The QED score showed a 30.1% improvement (from 0.73 to 0.95) for Top-1 and a 21.9% improvement (from 0.73 to 0.89) for Top-8000, compared with the training dataset. Furthermore, the generated molecules of InstGAN with logP and SA as the desired properties exhibited a notable improvement, with logP scores increasing by 78.6% for Top-1 and 76.8%, as well as 67.9% for SA scores for Top-8000, respectively. In multi-property optimization, InstGAN generated molecules with higher QED scores, compared with other baselines. Especially, InstGAN improved the QED score of the Top-1000 by 9.4%, comparing to the SOTA D2L-OMP baseline. Additionally, the generated molecules of InstGAN demonstrated substantial improvements, with the scores increasing by 30.1%, 78.6%, and 78.6% for Top-1, and 17.8%, 32.1%, and 64.3% for Top-8000, compared with the training dataset. Overall, InstGAN showcased substantial enhancements in both single- and multi-property optimization, underscoring its effectiveness in improving targeted chemical properties.

Figures D.1 and D.2 in the appendix show the top-ranked (Top-1) molecular structures generated by InstGAN in the single- and multi-property optimization tasks, respectively. The generated molecule adhered to Hückel’s rules (Klein & Trinajstić, 1984), essential for obtaining the targeted chemical properties of new drugs. These findings suggest that InstGAN successfully produced new drug-like molecules with relatively high QED, logP, and SA scores.

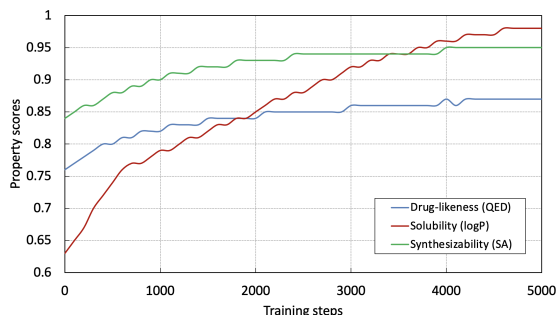


Figure 2. Trends in chemical properties of molecules generated during single-property optimization training.

Figure 2 and Fig. D.3 in the appendix depict the curves of average chemical property values versus training steps for molecules generated in single- and multi-property optimization tasks. Chemical properties for both single- and multi-property optimization exhibited gradual increases over 5000 training steps. In single-property optimization, the independence of the three chemical properties resulted in distinct and noticeable score increases. However, during the multi-property optimization process, the mutual constraints between properties led to similar changing trends in the values of the three properties.

Figure D.4 and Fig. 3 show the property distributions of molecules generated with single- and multi-property optimization, respectively. Intuitively, in comparison to the molecule distributions in the training set (in blue), the chemical property distributions of the newly generated molecules (in green) shifted to the right overall. This suggests that InstGAN produced a greater number of new molecules with desirable properties. Furthermore, the property scores of molecules generated through multi-property optimization were marginally lower than those from single-property optimization. This difference arises because InstGAN had to concurrently consider the enhancement of three properties (i.e., QED, logP, and SA) during multi-property optimization. In essence, multi-property optimization for molecular generation proves to be more challenging and intricate. Thus, the results demonstrated the effectiveness of InstGAN in desired chemical property optimization.

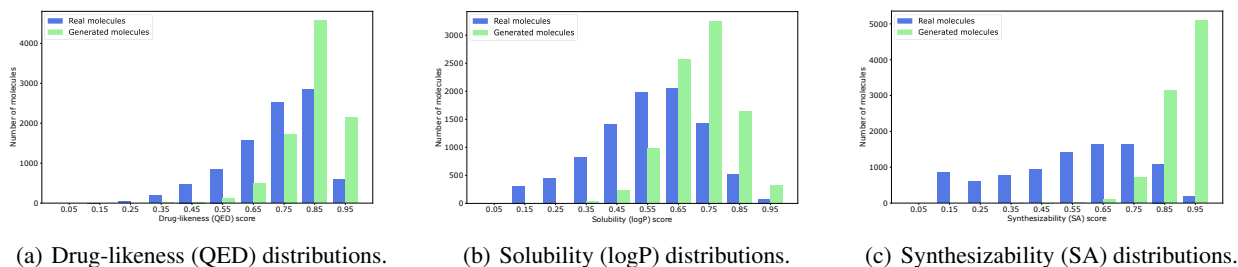


Figure 3. Property distributions of generated molecules with multi-property optimization.

Table 4. Effect of different variants of InstGAN.

|                | Validity     | Uniqueness   | Novelty      | Total        |
|----------------|--------------|--------------|--------------|--------------|
| w/o IR         | 97.80        | 70.71        | 98.02        | 67.79        |
| w/o GR         | 95.96        | 98.72        | 99.66        | 94.41        |
| w/o MIE        | 98.39        | 96.50        | 99.54        | 94.51        |
| <b>InstGAN</b> | <b>97.56</b> | <b>98.47</b> | <b>99.73</b> | <b>95.81</b> |

tion.

### 4.3. Ablation Studies

Table 4 demonstrates the impact of various InstGAN variants on molecular generation performance. During the training process of InstGAN, we excluded GR, and MIE individually to create three distinct variants, namely, “w/o IR,” “w/o GR,” and “w/o MIE.” These variants were then compared with InstGAN. In the “w/o IR” scenario, the calculation of instant reward was substituted with the MCTS RL algorithm. While MCTS enhanced GAN training stability with its extensive sampling, resulting in relatively high validity (97.80%), its computational complexity, stemming from the large number of samples, constrains its applicability in lengthy sequences. In the case of “w/o GR,” the validity was the lowest (95.96%, compared to 97.56% of InstGAN). Given that the GR involves the global information of a SMILES string, it provides additional sequence-related information for generating subsequent tokens in the molecular auto-regression process, thereby contributing to the validity improvement. MIE, by smoothing the probabilities of generating tokens, enhances diversity in sampling tokens with non-maximum probabilities. Consequently, in the “w/o MIE” scenario, the generated molecular distribution exhibited the lowest uniqueness (96.50%, compared to 98.47% of InstGAN). InstGAN, incorporating IR, GR, and MIE, showcased high validity, uniqueness, and Novelty scores, and achieved the highest total score of 95.81%.

Additionally, Tables E.1, E.2, E.3, and E.4 display the effects of  $\lambda$  on the performance. Overall, InstGAN can be applied to extensive chemical databases, optimizing chemical properties while retaining a low computational cost.

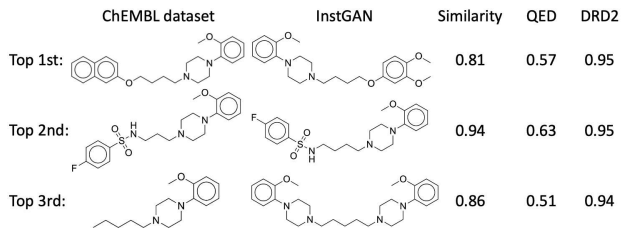


Figure 4. Comparison of the generated molecules with high DRD2 scores and similar approved drugs.

### 4.4. Case Studies

In the case studies, our goal is to generate molecules with high QED and a significant affinity for DRD2 within the ChEMBL database. This pursuit is critical for identifying potential drug candidates distinguished by enhanced drug-like properties and targeted therapeutic effects. This significance is underscored by the wealth of available experimental bioactive data, providing a robust foundation for advancing promising compounds in drug discovery.

Table F.1 in Appendix F assesses the performance of QED and DRD2 properties, demonstrating that the QED and DRD2 scores change with the corresponding weights. Furthermore, InstGAN enhanced the bioactivity of the generated molecules to 97.21%. Additionally, we selected a QED and DRD2 weight ratio of (0.3, 0.7) and generated bioactive molecules. Figure 4 compares the generated molecules with high DRD2 scores to similar approved drugs. These Top-3 molecules generated by InstGAN have high QED and DRD2 scores and are highly similar to approved drugs in the ChEMBL database, proving the effectiveness of InstGAN.

## 5. Conclusion

This study introduced InstGAN for generating molecules with multi-property optimization from scratch. Unlike MCTS RL algorithms, we employed an actor-critic RL algorithm for the efficient computation of IR and GR, resulting in reduced computation time and stabilized molecular



generation quality. Additionally, the inclusion of MIE was used to alleviate the mode collapse problem and promote diversity in molecular generation. The experimental results demonstrated that InstGAN achieves comparable performance to SOTA baseline models and efficiently generates molecules with single- and multi-property optimization.

InstGAN has two main limitations. First, the number of critics increases with the number of chemical properties that need to be optimized, which leads to an increase in the training cost. Second, the inclusion of additional hyperparameters, such as  $\lambda$  and  $W_{C_i}$ , requires manual tuning, posing a challenge for fine-tuning. In future work, we will explore solutions to address these challenges.

## Impact Statements

This paper presents work whose goal is to advance the field of Machine Learning. There are many potential societal consequences of our work, none which we feel must be specifically highlighted here.

## References

- Barshatski, G. and Radinsky, K. Unpaired generative molecule-to-molecule translation for lead optimization. In *Proceedings of the 27th ACM SIGKDD Conference on Knowledge Discovery & Data Mining*, pp. 2554–2564, 2021.
- Barshatski, G., Nordon, G., and Radinsky, K. Multi-property molecular optimization using an integrated poly-cycle architecture. In *Proceedings of the 30th ACM International Conference on Information & Knowledge Management*, pp. 3727–3736, 2021.
- Bickerton, G. R., Paolini, G. V., Besnard, J., Muresan, S., and Hopkins, A. L. Quantifying the chemical beauty of drugs. *Nature Chemistry*, 4(2):90–98, 2012.
- Cereto-Massagué, A., Ojeda, M. J., Valls, C., Mulero, M., Garcia-Vallvé, S., and Pujadas, G. Molecular fingerprint similarity search in virtual screening. *Methods*, 71:58–63, 2015.
- Chan, H. S., Shan, H., Dahoun, T., Vogel, H., and Yuan, S. Advancing drug discovery via artificial intelligence. *Trends in Pharmacological Sciences*, 40(8):592–604, 2019.
- Chen, H., Engkvist, O., Wang, Y., Olivecrona, M., and Blaschke, T. The rise of deep learning in drug discovery. *Drug Discovery Today*, 23(6):1241–1250, 2018.
- Comer, J. and Tam, K. Lipophilicity profiles: theory and measurement. *Pharmacokinetic Optimization in Drug Research: Biological, Physicochemical and Computational Strategies*, pp. 275–304, 2001.
- Dai, H., Dai, B., and Song, L. Discriminative embeddings of latent variable models for structured data. In *Proceedings of the International Conference on Machine Learning*, pp. 2702–2711. PMLR, 2016.
- Dai, H., Tian, Y., Dai, B., Skiena, S., and Song, L. Syntax-directed variational autoencoder for molecule generation. In *Proceedings of the International Conference on Learning Representations*, 2018.
- De Cao, N. and Kipf, T. MolGAN: An implicit generative model for small molecular graphs. *ArXiv Preprint ArXiv:1805.11973*, 2018.
- de Masson d’Autume, C., Mohamed, S., Rosca, M., and Rae, J. Training language GANs from scratch. In *Proceedings of the Advances in Neural Information Processing Systems*, volume 32, 2019.
- Dollar, O., Joshi, N., Beck, D. A., and Pfandtner, J. Attention-based generative models for de novo molecular design. *Chemical Science*, 12(24):8362–8372, 2021.
- Ertl, P. and Schuffenhauer, A. Estimation of synthetic accessibility score of drug-like molecules based on molecular complexity and fragment contributions. *Journal of Cheminformatics*, 1(1):1–11, 2009.
- Fedus, W., Goodfellow, I., and Dai, A. M. MaskGAN: better text generation via filling in the\_. *ArXiv Preprint ArXiv:1801.07736*, 2018.
- Gaulton, A., Bellis, L. J., Bento, A. P., Chambers, J., Davies, M., Hersey, A., Light, Y., McGlinchey, S., Michalovich, D., Al-Lazikani, B., et al. ChEMBL: a large-scale bioactivity database for drug discovery. *Nucleic Acids Research*, 40(D1):D1100–D1107, 2012.
- Gaulton, A., Hersey, A., Nowotka, M., Bento, A. P., Chambers, J., Mendez, D., Motowo, P., Atkinson, F., Bellis, L. J., Cibrián-Uhalte, E., et al. The ChEMBL database in 2017. *Nucleic Acids Research*, 45(D1):D945–D954, 2017.
- Gilmer, J., Schoenholz, S. S., Riley, P. F., Vinyals, O., and Dahl, G. E. Neural message passing for quantum chemistry. In *Proceedings of the International Conference on Machine Learning*, pp. 1263–1272. PMLR, 2017.
- Goodfellow, I., Pouget-Abadie, J., Mirza, M., Xu, B., Warde-Farley, D., Ozair, S., Courville, A., and Bengio, Y. Generative adversarial nets. In *Proceedings of the Advances in Neural Information Processing Systems*, volume 27, 2014.

- Guimaraes, G. L., Sanchez-Lengeling, B., Outeiral, C., Farias, P. L. C., and Aspuru-Guzik, A. Objective-reinforced generative adversarial networks (ORGAN) for sequence generation models. *ArXiv Preprint ArXiv:1705.10843*, 2017.
- Guo, S., Guan, J., and Zhou, S. Diffusing on two levels and optimizing for multiple properties: A novel approach to generating molecules with desirable properties. *ArXiv Preprint ArXiv:2310.04463*, 2023.
- Irwin, J. J., Sterling, T., Mysinger, M. M., Bolstad, E. S., and Coleman, R. G. Zinc: a free tool to discover chemistry for biology. *Journal of Chemical Information and Modeling*, 52(7):1757–1768, 2012.
- Jin, W., Barzilay, R., and Jaakkola, T. Junction tree variational autoencoder for molecular graph generation. In *Proceedings of the International Conference on Machine Learning*, pp. 2323–2332. PMLR, 2018.
- Jin, W., Barzilay, R., and Jaakkola, T. Hierarchical graph-to-graph translation for molecules. *ArXiv Preprint ArXiv:1907.11223*, 2019.
- Jo, J., Lee, S., and Hwang, S. J. Score-based generative modeling of graphs via the system of stochastic differential equations. In *Proceedings of the International Conference on Machine Learning*, pp. 10362–10383. PMLR, 2022.
- Kingma, D. P. and Dhariwal, P. GLow: Generative flow with invertible 1x1 convolutions. In *Proceedings of the Advances in Neural Information Processing Systems*, volume 31, 2018.
- Klein, D. and Trinajstić, N. Hückel rules and electron correlation. *Journal of the American Chemical Society*, 106(26):8050–8056, 1984.
- Konda, V. and Tsitsiklis, J. Actor-critic algorithms. In *Proceedings of the Advances in Neural Information Processing Systems*, volume 12, 1999.
- Kusner, M. J., Paige, B., and Hernández-Lobato, J. M. Grammar variational autoencoder. In *Proceedings of the International Conference on Machine Learning*, pp. 1945–1954. PMLR, 2017.
- Landrum, G. Rdkit documentation. *Release*, 1(1-79):4, 2013.
- Li, C. and Yamanishi, Y. SpotGAN: A reverse-transformer gan generates scaffold-constrained molecules with property optimization. In *Proceedings of the Joint European Conference on Machine Learning and Knowledge Discovery in Databases*, pp. 323–338. Springer, 2023.
- Li, C., Yamanaka, C., Kaitoh, K., and Yamanishi, Y. Transformer-based objective-reinforced generative adversarial network to generate desired molecules. In *Proceedings of the Thirty-First International Joint Conference on Artificial Intelligence, IJCAI-22*, pp. 3884–3890, 2022.
- Lippe, P. and Gavves, E. Categorical normalizing flows via continuous transformations. In *Proceedings of the International Conference on Learning Representations*, 2021.
- Luo, Y., Yan, K., and Ji, S. GraphDF: A discrete flow model for molecular graph generation. In *Proceedings of the International Conference on Machine Learning*, pp. 7192–7203. PMLR, 2021.
- Olivecrona, M., Blaschke, T., Engkvist, O., and Chen, H. Molecular de-novo design through deep reinforcement learning. *Journal of Cheminformatics*, 9(1):1–14, 2017.
- OpenAI, R. GPT-4 technical report. arxiv 2303.08774. *View in Article*, 2023.
- Paul, D., Sanap, G., Shenoy, S., Kalyane, D., Kalia, K., and Tekade, R. K. Artificial intelligence in drug discovery and development. *Drug Discovery Today*, 26(1):80, 2021.
- Rogers, D. J. and Tanimoto, T. T. A computer program for classifying plants. *Science*, 132(3434):1115–1118, 1960.
- Shi, C., Xu, M., Zhu, Z., Zhang, W., Zhang, M., and Tang, J. GraphAF: a flow-based autoregressive model for molecular graph generation. *ArXiv Preprint ArXiv:2001.09382*, 2020.
- Sutton, R. S. and Barto, A. G. *Reinforcement learning: An introduction*. MIT press, 2018.
- Tang, H., Li, C., Jiang, S., Yu, H., Kamei, S., Yamanishi, Y., and Morimoto, Y. Earlgan: An enhanced actor-critic reinforcement learning agent-driven gan for de novo drug design. *Pattern Recognition Letters*, 175:45–51, 2023.
- Vignac, C., Krawczuk, I., Siraudin, A., Wang, B., Cevher, V., and Frossard, P. DiGress: Discrete denoising diffusion for graph generation. In *Proceedings of the 11th International Conference on Learning Representations*, 2023.
- Weininger, D. SMILES, a chemical language and information system. 1. introduction to methodology and encoding rules. *Journal of Chemical Information and Computer Sciences*, 28(1):31–36, 1988.

Williams, R. J. Simple statistical gradient-following algorithms for connectionist reinforcement learning. *Machine Learning*, 8:229–256, 1992.

Yu, L., Zhang, W., Wang, J., and Yu, Y. SeqGAN: Sequence generative adversarial nets with policy gradient. In *Proceedings of the AAAI Conference on Artificial Intelligence*, volume 31, 2017.

Zang, C. and Wang, F. MoFlow: an invertible flow model for generating molecular graphs. In *Proceedings of the 26th ACM SIGKDD International Conference on Knowledge Discovery & Data Mining*, pp. 617–626, 2020.

Zhang, S., Kang, N., Ryder, T., and Li, Z. Iflow: Numerically invertible flows for efficient lossless compression via a uniform coder. In *Proceedings of the Advances in Neural Information Processing Systems*, volume 34, pp. 5822–5833, 2021.

# Supplementary Material

## Molecular Generative Adversarial Network with Multi-Property Optimization

### A. Detailed Model Description

#### A.1. Details of Generator

Recurrent neural networks (RNNs) have demonstrated versatility in handling both input and output sequence data. When presented with an input vector at time step  $t$ ,  $\mathbf{S}_{1:t} = [s_1, \dots, s_t]$ , and the corresponding output vector  $\tilde{\mathbf{S}}_{1:t} = [\tilde{s}_1, \dots, \tilde{s}_t]$ , the objective of the RNNs is to model the distribution  $p(\tilde{s}_t | s_1, s_2, \dots, s_t)$ . These networks operate as dynamic systems, as illustrated in Fig. 1 (a), where the RNNs state at any  $t$ -th time step (i.e., any  $t$ -th position in the SMILES string) relies on the previous observations.

For a given input SMILES string, the generative RNNs undergo training to extend this SMILES string by predicting the subsequent sequence token, denoted as  $\tilde{s}(t) = s_t$ . In this study, RNNs equipped with LSTM cells are utilized, a choice made to address challenges like vanishing and exploding gradient problems associated with extended sequences and a substantial network architecture. At each time step  $t$ , such a network is delineated by the subsequent set of equations:

$$\mathbf{i}_t = \sigma(\mathbf{W}_{si}s_t + \mathbf{W}_{hi}\mathbf{h}_{t-1} + \mathbf{b}_i), \quad (11)$$

$$\mathbf{f}_t = \sigma(\mathbf{W}_{sf}s_t + \mathbf{W}_{hf}\mathbf{h}_{t-1} + \mathbf{b}_f), \quad (12)$$

$$\mathbf{o}_t = \sigma(\mathbf{W}_{so}s_t + \mathbf{W}_{ho}\mathbf{h}_{t-1} + \mathbf{b}_o), \quad (13)$$

$$\tilde{\mathbf{c}}_t = \tanh(\mathbf{W}_{sc}s_t + \mathbf{W}_{hc}\mathbf{h}_{t-1} + \mathbf{b}_c), \quad (14)$$

$$\mathbf{c}_t = \mathbf{f}_t\mathbf{c}_{t-1} + \mathbf{i}_t\tilde{\mathbf{c}}_t, \quad (15)$$

$$\mathbf{h}_t = \mathbf{o}_t \tanh(\mathbf{c}_t). \quad (16)$$

Here, the vectors  $\mathbf{i}_t$ ,  $\mathbf{f}_t$ , and  $\mathbf{o}_t$  denote the input, forget, and output gate vectors, respectively. These vectors are outcomes of the sigmoid activation function, indicating values between 0 and 1.  $\mathbf{c}_t$  is a vector responsible for preserving long-term memory. The output vector  $\mathbf{y}_t$  is ultimately computed as follows:

$$\tilde{s}_t = g(\mathbf{W}_{hs}\mathbf{h}_t), \quad (17)$$

where  $g(\cdot)$  represents a nonlinear activation function.

The common approach for RNNs in SMILES string generation typically follows a left-to-right (forward) direction, covering the range from  $t = 1$  to  $t = T$ , where  $T$  represents the length of a SMILES string. In the training phase, the initial position of the input is filled with a start-of-sequence token (“<SOS>”), and the final position is filled with an end-of-sequence token. New sequences are generated by (1) inputting the starting token (“<SOS>”), and (2) iteratively selecting the subsequent token as the model progresses through the previous sequence of tokens until the end token (“<EOS>”) is produced. At each time step  $t$ , the probability for each  $v$ -th token to follow the preceding portion of the generated string is computed using a softmax function. The calculation is outlined as follows:

$$p(s_{t+1} = v | s_1, s_2, \dots, s_t) = \frac{\exp(\tilde{s}_t^v / \text{Temp})}{\sum_{i=1}^V \exp(\tilde{s}_t^i / \text{Temp})}. \quad (18)$$

Here,  $\tilde{s}_t^v$  signifies the model output (logits) for the  $v$ -th token at time  $t$ , with  $v$  ranging over the set  $V$  that encompasses all tokens. The selection of tokens is governed by the temperature parameter Temp. At higher temperatures, all tokens demonstrate nearly identical probabilities; as the temperature decreases, the predicted  $\tilde{s}_t^v$  progressively influences the probability of the  $v$ -th token. With a lower temperature, the probability of the token with the highest  $\tilde{s}_t^v$  approaches 1.



## A.2. Details of Discriminator

A bidirectional LSTM (Bi-LSTM) serves as a powerful discriminator to assess the authenticity and quality of SMILES strings at the token-level. Unlike traditional LSTMs, the Bi-LSTM processes input SMILES strings in both forward and backward directions, enabling a comprehensive understanding of contextual information.

The calculations in a Bi-LSTM involve two separate LSTM networks, one processing the sequence from the beginning to the end (forward LSTM), and the other processing it in reverse (backward LSTM). The hidden states from both LSTMs are concatenated at each time step, providing a more nuanced representation of the sequence. The calculation is as follows:

$$\mathbf{i}_t = \sigma(\mathbf{W}_{ii}s_t + \mathbf{W}_{hi}\vec{\mathbf{h}}_{t-1} + \mathbf{b}_{ii} + \mathbf{b}_{hi}), \quad (19)$$

$$\mathbf{f}_t = \sigma(\mathbf{W}_{if}s_t + \mathbf{W}_{hf}\vec{\mathbf{h}}_{t-1} + \mathbf{b}_{if} + \mathbf{b}_{hf}), \quad (20)$$

$$\mathbf{o}_t = \sigma(\mathbf{W}_{io}s_t + \mathbf{W}_{ho}\vec{\mathbf{h}}_{t-1} + \mathbf{b}_{io} + \mathbf{b}_{ho}), \quad (21)$$

$$\tilde{\mathbf{c}}_t = \tanh(\mathbf{W}_{ic}s_t + \mathbf{W}_{hc}\vec{\mathbf{h}}_{t-1} + \mathbf{b}_{ic} + \mathbf{b}_{hc}), \quad (22)$$

$$\mathbf{c}_t = \mathbf{f}_t\mathbf{c}_{t-1} + \mathbf{i}_t\tilde{\mathbf{c}}_t, \quad (23)$$

$$\mathbf{h}_t = \mathbf{o}_t\tanh(\mathbf{c}_t). \quad (24)$$

The backward LSTM computes hidden states ( $\overleftarrow{\mathbf{h}}_t$ ) using similar equations with parameters specific to the backward pass. Finally, the hidden states from both LSTMs are concatenated to obtain the final hidden state  $\mathbf{h}_t = [\vec{\mathbf{h}}_t, \overleftarrow{\mathbf{h}}_t]$ , which is used for discrimination purposes. This Bi-LSTM approach facilitates a more robust understanding of the sequential information, enhancing the discriminator’s ability to assess the quality and authenticity of the input SMILES strings.

## B. Chemical Properties and Evaluation Metrics

### B.1. Details of Chemical Properties

**Drug-likeness (QED) calculation.** The QED score is determined through a weighted average of eight molecular descriptors: molecular weight (MW), octanol-water partition coefficient (ALOGP), number of hydrogen bond donors (HBDs), number of hydrogen bond acceptors (HBAs), molecular polar surface area (PSA), number of rotatable bonds (ROTBs), number of aromatic rings (AROMs), and number of structural alerts (ALERTS). The QED can be calculated as follows:

$$\text{QED} = \exp\left(\frac{\sum_{i=1}^8 W_i \ln d_i}{\sum_{i=1}^8 W_i}\right), \quad (25)$$

where  $d_i$  denotes the desirability function, and  $W_i$  represents the  $i$ -th descriptor.

**Solubility (logP) calculation.** Solubility is computed using logP, where P is the partition coefficient defined as the ratio of the concentrations of a molecule on an octanol-water surface. The logP can be calculated as follows:

$$\log P = \log \frac{c_o}{c_w}, \quad (26)$$

where  $c_o$  and  $c_w$  represent the organic and water-phase substance activity, respectively.

**Synthesizability (SA) calculation.** Typically, Synthesizability is computed using the SA score, which assesses the ease of synthesizing a molecule. The calculation is shown as below:

$$\text{SA} = r_s - \sum_{i=1}^5 p_i, \quad (27)$$

where  $r_s$  represents the synthetic molecule’s knowledge analysis, which is the ratio of the summed fragments’ contributions to all fragment numbers within the molecule, utilizing experimental results from the literature (Li & Yamanishi, 2023).  $p_i$  ( $i \in 1, \dots, 5$ ) is the ring complexity, stereo complexity, macrocycle penalty, size penalty, and bridge penalty.

**Dopamine Receptor D2 (DRD2) calculation.** The DRD2 score quantifies the likelihood of interaction between a molecule and a target protein (Olivecrona et al., 2017). We selected DRD2 as the target protein and utilized a random forest classifier from the Scikit-learn toolkit for computation. Specifically, we initially gathered DRD2-molecule interaction data from the ChEMBL30 dataset (accessed on 2022-03-17) (Gaulton et al., 2012). Subsequently, we employed the Ki values (unit: nmol/L) from ChEMBL217 as the interaction data. After eliminating missing values and duplicate molecules, we obtained a dataset of 6652 molecule-Ki pairs. To construct the model, we trained 500 decision-tree classifiers using the random forest classifier for binary classification. The input to the classifier was the SMILES representation of a molecule, which was then transformed into a 2048-dimensional ECFP4 (extended connectivity fingerprint, up to four bonds). The labels for the binary classifier were defined as follows:

$$\text{label} = \begin{cases} 0 & \text{if } 9 - \log \text{Ki} > 7, \\ 1 & \text{otherwise.} \end{cases}$$

Then, the classifier’s output is determined by computing the predicted probability associated with the label of 1, representing the DRD2 score.

Note that higher scores for these properties indicate greater desirability. The QED score ranges from 0 to 1, and the logP and SA scores range from 0.1 to 1. The RDKit tool was utilized for implementation.

## B.2. Details of Evaluation Metrics

Following the evaluation criteria in (Li & Yamanishi, 2023), we consider the validity, uniqueness, novelty, total, and diversity.

**Validity.** Validity is the ratio of chemically valid SMILES to all generated SMILES. The calculation is as follows:

$$\text{Validity} = \frac{N_{\mathcal{D}_V}}{N_{\mathcal{D}_G}}, \quad (28)$$

where  $N_{\mathcal{D}_G}$  is the number of generated SMILES-like strings, and  $N_{\mathcal{D}_V}$  is the number of generated chemically valid SMILES strings.

**Uniqueness.** Uniqueness is determined by the ratio of chemically valid and unique SMILES strings to the number of valid SMILES strings, which is calculated by

$$\text{Uniqueness} = \frac{N_{\mathcal{D}_U}}{N_{\mathcal{D}_V}}, \quad (29)$$

where  $N_{\mathcal{D}_U}$  denotes the number of generated chemically valid and unique SMILES strings.

**Novelty.** Novelty is the ratio of chemically valid, unique, and previously unseen SMILES strings to all chemically valid and unique SMILES. The mathematical definition is as follows:

$$\text{Novelty} = \frac{N_{\mathcal{D}_N}}{N_{\mathcal{D}_U}}, \quad (30)$$

where  $N_{\mathcal{D}_N}$  is the number of generated chemically valid and unique SMILES strings that are absent from the training dataset.

**Total.** The Total score is defined as the ratio of novel molecules to all generated ones. The formula is as follows:

$$\text{Total} = \frac{N_{\mathcal{D}_N}}{N_{\mathcal{D}_G}}. \quad (31)$$

**Diversity.** The diversity is also used to evaluate the *diversity* of novel SMILES strings  $\mathcal{D}_N$ , which is computed based on Tanimoto coefficient (Rogers & Tanimoto, 1960) of Morgan fingerprint (Cereto-Massagué et al., 2015). The mean diversity

$Div(\mathcal{M}_N)$  and Tanimoto similarity  $Sim(m_i, m_j)$  are defined as follows:

$$Div(\mathcal{M}_N) = 1 - \frac{1}{|\mathcal{M}_N|} \sum_{m_i, m_j \in \mathcal{M}_N} Sim(m_i, m_j), \quad (32)$$

and

$$Sim(m_i, m_j) = \frac{|m_i \& m_j|}{|m_i| + |m_j| - |m_i \& m_j|}. \quad (33)$$

Here, the scores are calculated based on the Morgan fingerprints ( $m_i$  and  $m_j$ ) of two arbitrarily generated novel molecules. The resulting scores range from 0 to 1, with higher values indicating better diversity. The RDKit tool was utilized for the implementation.

### C. Average of Multiple Pretraining

Table C.1. Average results obtained from multiple pretraining of InstGAN.

|         | Validity (%) $\uparrow$ | Uniqueness (%) $\uparrow$ | Novelty (%) $\uparrow$ | Diversity $\uparrow$ | QED $\uparrow$ | logP $\uparrow$ | SA $\uparrow$ |
|---------|-------------------------|---------------------------|------------------------|----------------------|----------------|-----------------|---------------|
| 1       | 96.25                   | 98.64                     | 99.68                  | 0.90                 | 0.76           | 0.62            | 0.84          |
| 2       | 94.67                   | 98.69                     | 99.73                  | 0.90                 | 0.79           | 0.63            | 0.84          |
| 3       | 95.42                   | 98.55                     | 99.73                  | 0.90                 | 0.75           | 0.62            | 0.83          |
| Average | 95.45                   | 98.63                     | 99.71                  | 0.90                 | 0.77           | 0.62            | 0.84          |

### D. Details of Property Optimization

Table D.1. Single- and multi-property assessment of the top-k generated molecules using InstGAN.

|         | Chemical Property      | Top-1 | Top-1000 | Top-2000 | Top-4000 | Top-6000 | Top-8000 |
|---------|------------------------|-------|----------|----------|----------|----------|----------|
| InstGAN | Single property (QED)  | 0.95  | 0.94     | 0.93     | 0.92     | 0.91     | 0.89     |
|         | Single property (logP) | 1.00  | 1.00     | 1.00     | 1.00     | 1.00     | 0.99     |
|         | Single property (SA)   | 1.00  | 1.00     | 0.99     | 0.97     | 0.95     | 0.94     |
|         | Multi-property (QED)   | 0.95  | 0.93     | 0.92     | 0.90     | 0.88     | 0.86     |
|         | Multi-property (logP)  | 1.00  | 0.89     | 0.85     | 0.81     | 0.78     | 0.74     |
|         | Multi-property (SA)    | 1.00  | 0.99     | 0.98     | 0.96     | 0.94     | 0.92     |

Figure D.1 shows the Top-1 generated molecular structures by InstGAN in single-property optimization exhibited the highest QED, logP, and SA scores.

### E. Details of Ablation Studies

Tables E.1, E.2, E.3, and E.4 display the effects of  $\lambda$  on the performance.

### F. Details of Case Studies

Table F.1 assesses the performance of QED and DRD2 properties, demonstrating that the QED and DRD2 scores change with the corresponding weights. Furthermore, InstGAN enhanced the bioactivity of the generated molecules to 97.21%. Additionally, we selected a QED and DRD2 weight ratio of (0.3, 0.7) and generated bioactive molecules. Figure 4 compares the generated molecules with high DRD2 scores to similar approved drugs. These Top-3 molecules generated by InstGAN have high QED and DRD2 scores and are highly similar to approved drugs in the ChEMBL database, proving the effectiveness of InstGAN.

Table E.1. Effect of  $\lambda$  on the performance of single-property optimization (QED) for the ZINC dataset.

| $\lambda$ | QED $\uparrow$ | Validity (%) $\uparrow$ | Uniqueness (%) $\uparrow$ | Novelty (%) $\uparrow$ | Diversity $\uparrow$ | logP $\uparrow$ | SA $\uparrow$ | Time (h) $\downarrow$ |
|-----------|----------------|-------------------------|---------------------------|------------------------|----------------------|-----------------|---------------|-----------------------|
| 0.0       | 0.77           | 94.73                   | 98.89                     | 99.72                  | 0.90                 | 0.60            | 0.81          | 3.73                  |
| 0.1       | 0.79           | 95.62                   | 99.11                     | 99.83                  | 0.90                 | 0.60            | 0.81          | 3.89                  |
| 0.2       | 0.81           | 97.05                   | 98.76                     | 99.74                  | 0.90                 | 0.60            | 0.82          | 3.87                  |
| 0.3       | 0.83           | 97.89                   | 98.31                     | 99.69                  | 0.89                 | 0.60            | 0.83          | 3.83                  |
| 0.4       | 0.85           | 97.96                   | 97.24                     | 99.55                  | 0.89                 | 0.61            | 0.84          | 3.85                  |
| 0.5       | 0.87           | 98.52                   | 94.24                     | 99.56                  | 0.88                 | 0.61            | 0.86          | 3.81                  |
| 0.6       | 0.87           | 98.90                   | 91.87                     | 99.57                  | 0.88                 | 0.61            | 0.87          | 3.71                  |
| 0.7       | 0.87           | 98.69                   | 92.09                     | 99.57                  | 0.88                 | 0.62            | 0.87          | 3.56                  |
| 0.8       | 0.86           | 98.61                   | 92.01                     | 99.67                  | 0.88                 | 0.62            | 0.88          | 3.38                  |
| 0.9       | 0.86           | 98.53                   | 92.01                     | 99.56                  | 0.88                 | 0.62            | 0.88          | 2.91                  |
| 1.0       | 0.86           | 98.34                   | 91.95                     | 99.61                  | 0.88                 | 0.62            | 0.88          | 2.79                  |

Table E.2. Effect of  $\lambda$  on the performance of single-property optimization (logP) for the ZINC dataset.

| $\lambda$ | logP $\uparrow$ | Validity (%) $\uparrow$ | Uniqueness (%) $\uparrow$ | Novelty (%) $\uparrow$ | Diversity $\uparrow$ | QED $\uparrow$ | SA $\uparrow$ | Time (h) $\downarrow$ |
|-----------|-----------------|-------------------------|---------------------------|------------------------|----------------------|----------------|---------------|-----------------------|
| 0.0       | 0.63            | 96.26                   | 98.70                     | 99.73                  | 0.90                 | 0.76           | 0.84          | 3.49                  |
| 0.1       | 0.66            | 95.06                   | 99.16                     | 99.78                  | 0.90                 | 0.76           | 0.81          | 3.53                  |
| 0.2       | 0.71            | 95.45                   | 99.43                     | 99.83                  | 0.90                 | 0.74           | 0.82          | 3.39                  |
| 0.3       | 0.78            | 95.78                   | 99.32                     | 99.87                  | 0.90                 | 0.71           | 0.82          | 3.50                  |
| 0.4       | 0.90            | 96.36                   | 97.77                     | 99.97                  | 0.89                 | 0.62           | 0.82          | 3.43                  |
| 0.5       | 0.97            | 97.18                   | 92.80                     | 100.00                 | 0.88                 | 0.50           | 0.78          | 3.45                  |
| 0.6       | 0.95            | 94.71                   | 95.20                     | 99.94                  | 0.89                 | 0.52           | 0.78          | 3.03                  |
| 0.7       | 0.93            | 94.42                   | 95.92                     | 99.98                  | 0.90                 | 0.53           | 0.78          | 2.74                  |
| 0.8       | 0.91            | 92.35                   | 97.86                     | 99.97                  | 0.90                 | 0.57           | 0.79          | 2.50                  |
| 0.9       | 0.88            | 91.59                   | 98.50                     | 99.97                  | 0.90                 | 0.61           | 0.81          | 2.48                  |
| 1.0       | 0.92            | 93.18                   | 97.36                     | 99.93                  | 0.90                 | 0.55           | 0.80          | 2.41                  |



## Single property optimization

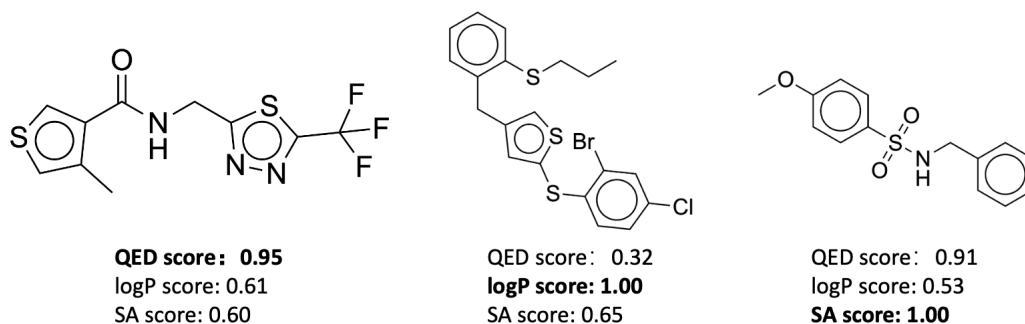


Figure D.1. The Top-1 generated molecular structures by InstGAN in single-property optimization exhibited the highest QED, logP, and SA scores.

## Multi-property optimization

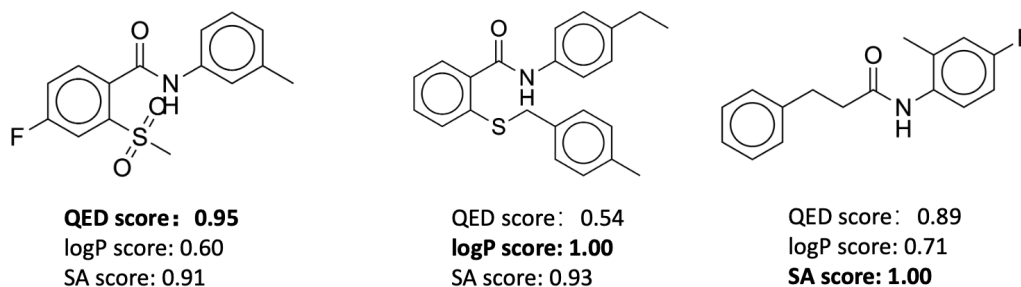


Figure D.2. The Top-1 molecular structures generated by InstGAN in multi-property optimization exhibited the highest QED, logP, and SA scores.

Table E.3. Effect of  $\lambda$  on the performance of single-property optimization (SA) for the ZINC dataset.

| $\lambda$ | SA $\uparrow$ | Validity (%) $\uparrow$ | Uniqueness (%) $\uparrow$ | Novelty (%) $\uparrow$ | Diversity $\uparrow$ | QED $\uparrow$ | logP $\uparrow$ | Time (h) $\downarrow$ |
|-----------|---------------|-------------------------|---------------------------|------------------------|----------------------|----------------|-----------------|-----------------------|
| 0.0       | 0.84          | 96.20                   | 98.73                     | 99.72                  | 0.90                 | 0.76           | 0.63            | 3.80                  |
| 0.1       | 0.84          | 96.20                   | 98.74                     | 99.72                  | 0.90                 | 0.76           | 0.63            | 3.79                  |
| 0.2       | 0.85          | 97.05                   | 98.50                     | 99.61                  | 0.89                 | 0.78           | 0.62            | 3.77                  |
| 0.3       | 0.88          | 97.96                   | 97.07                     | 99.62                  | 0.89                 | 0.79           | 0.62            | 3.75                  |
| 0.4       | 0.92          | 98.77                   | 91.89                     | 99.48                  | 0.88                 | 0.80           | 0.63            | 3.82                  |
| 0.5       | 0.92          | 98.55                   | 92.69                     | 99.47                  | 0.87                 | 0.79           | 0.62            | 3.44                  |
| 0.6       | 0.91          | 98.72                   | 93.25                     | 99.52                  | 0.88                 | 0.79           | 0.62            | 2.73                  |
| 0.7       | 0.92          | 98.52                   | 92.15                     | 99.47                  | 0.87                 | 0.79           | 0.63            | 2.29                  |
| 0.8       | 0.91          | 98.27                   | 94.03                     | 99.49                  | 0.88                 | 0.78           | 0.62            | 2.06                  |
| 0.9       | 0.91          | 98.39                   | 93.43                     | 99.55                  | 0.88                 | 0.79           | 0.63            | 1.94                  |
| 1         | 0.91          | 98.35                   | 93.25                     | 99.54                  | 0.88                 | 0.79           | 0.63            | 1.91                  |

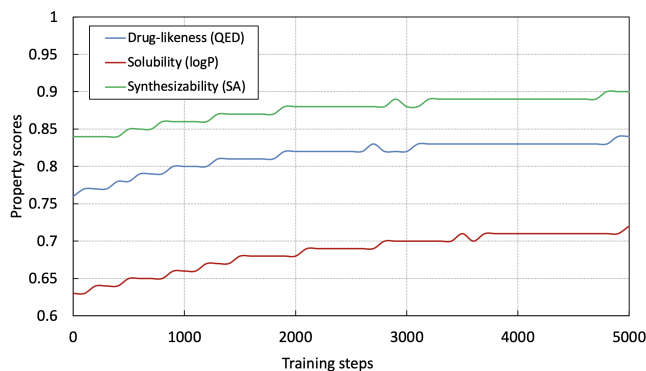
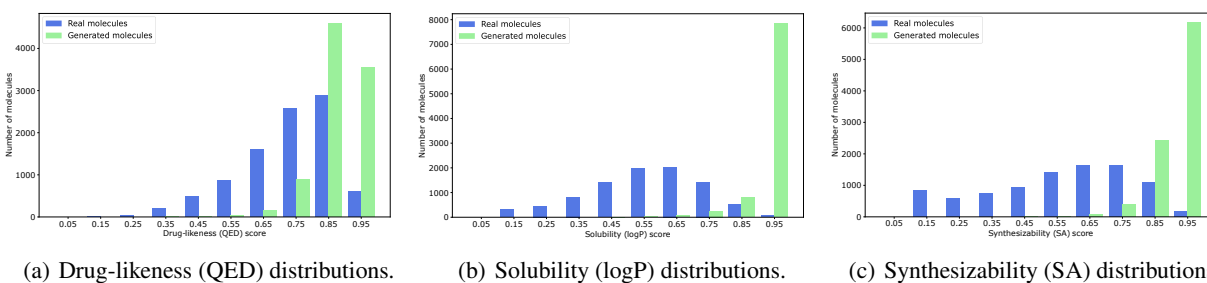


Figure D.3. Trends in chemical properties of molecules generated during multi-property optimization training.



(a) Drug-likeness (QED) distributions.

(b) Solubility (logP) distributions.

(c) Synthesizability (SA) distributions.

Figure D.4. Property distributions of generated molecules with single-property optimization.

 Table E.4. Effect of  $\lambda$  on the performance of multi-property optimization for the ZINC dataset.

| $\lambda$ | QED $\uparrow$ | logP $\uparrow$ | SA $\uparrow$ | Validity (%) $\uparrow$ | Uniqueness (%) $\uparrow$ | Novelty (%) $\uparrow$ | Diversity $\uparrow$ | Time (h) $\downarrow$ |
|-----------|----------------|-----------------|---------------|-------------------------|---------------------------|------------------------|----------------------|-----------------------|
| 0.0       | 0.76           | 0.63            | 0.84          | 95.89                   | 98.83                     | 99.68                  | 0.90                 | 4.36                  |
| 0.1       | 0.76           | 0.63            | 0.84          | 95.89                   | 98.83                     | 99.68                  | 0.90                 | 4.43                  |
| 0.2       | 0.79           | 0.64            | 0.83          | 96.93                   | 98.90                     | 99.81                  | 0.90                 | 4.46                  |
| 0.3       | 0.80           | 0.65            | 0.85          | 97.46                   | 98.63                     | 99.71                  | 0.89                 | 4.48                  |
| 0.4       | 0.82           | 0.68            | 0.87          | 98.25                   | 97.14                     | 99.55                  | 0.88                 | 4.50                  |
| 0.5       | 0.84           | 0.72            | 0.90          | 98.96                   | 92.25                     | 99.50                  | 0.87                 | 4.19                  |
| 0.6       | 0.84           | 0.72            | 0.91          | 99.18                   | 91.54                     | 99.66                  | 0.87                 | 4.14                  |
| 0.7       | 0.83           | 0.72            | 0.91          | 98.72                   | 91.73                     | 99.54                  | 0.87                 | 3.67                  |
| 0.8       | 0.83           | 0.72            | 0.92          | 98.70                   | 91.60                     | 99.56                  | 0.87                 | 3.38                  |
| 0.9       | 0.82           | 0.70            | 0.91          | 98.49                   | 92.65                     | 99.54                  | 0.88                 | 2.92                  |
| 1.0       | 0.82           | 0.70            | 0.91          | 98.40                   | 93.42                     | 99.53                  | 0.88                 | 2.78                  |

Table F.1. Effect of weights on QED and DRD2 property scores.

| Weight (QED, DRD2) | QED $\uparrow$ | DRD2 $\uparrow$ | Validity (%) $\uparrow$ | Uniqueness (%) $\uparrow$ | Novelty (%) $\uparrow$ |
|--------------------|----------------|-----------------|-------------------------|---------------------------|------------------------|
| Pretrain           | 0.70           | 0.21            | 94.87                   | 98.46                     | 99.13                  |
| (0.5, 0.5)         | 0.80           | 0.27            | 97.21                   | 87.52                     | 99.14                  |
| (0.4, 0.6)         | 0.78           | 0.28            | 97.17                   | 84.29                     | 99.05                  |
| (0.3, 0.7)         | 0.76           | 0.29            | 96.66                   | 84.80                     | 99.24                  |
| (0.2, 0.8)         | 0.73           | 0.30            | 96.25                   | 84.35                     | 99.47                  |
| (0.1, 0.9)         | 0.70           | 0.31            | 95.52                   | 85.49                     | 99.44                  |